THE ASTROPHYSICAL JOURNAL, 431:237–246, 1994 August 10

IONIZATION NEBULAE SURROUNDING SUPERSOFT X-RAY SOURCES

S. RAPPAPORT,[1] E. CHIANG,[1] T. KALLMAN,[2] AND R. MALINA[3]
Received 1993 December 13; accepted 1994 February 1

ABSTRACT

In this work we carry out a theoretical investigation of a new type of astrophysical gaseous nebula, viz., ionized regions surrounding supersoft X-ray sources. Supersoft X-ray sources, many of which have characteristic luminosities of $\sim 10^{37}$–10^{38} ergs s^{-1} and effective temperatures of $\sim 4 \times 10^5$ K, were first discovered with the *Einstein Observatory*. These sources have now been shown to constitute a distinct class of X-ray source and are being found in substantial numbers with *ROSAT*. We predict that these sources should be surrounded by regions of ionized hydrogen and helium with properties that are distinct from other astrophysical gaseous nebulae. We present calculations of the ionization and temperature structure of these ionization nebulae, as well as the expected optical line fluxes. The ionization profiles for both hydrogen and helium exhibit substantially more gradual transitions from the ionized to the unionized state than is the case for conventional H II regions. The calculated optical line intensities are presented as absolute fluxes from sources in the Large Magellanic Cloud and as fractions of the central source luminosity. We find, in particular, that [O III] λ5008 and He II λ4686 are especially prominent in these ionization nebulae as compared to other astrophysical nebulae. We propose that searches for supersoft X-rays via their characteristic optical lines may reveal sources in regions where the soft X-rays are nearly completely absorbed by the interstellar medium.

Subject headings: binaries: close — H II regions — ISM: general — H II regions — white dwarfs
X-rays: ISM

1. INTRODUCTION

In this work we carry out a theoretical investigation of a new type of astrophysical gaseous nebula, viz., ionized regions surrounding supersoft X-ray sources. Many of these sources have characteristic luminosities of $\sim 10^{37}$–10^{38} ergs s^{-1} and effective temperatures of ~ 2–6×10^5 K ($kT \simeq 17$–50 eV). Supersoft X-ray sources themselves are a new class of X-ray source that was originally discovered during a survey of the Large Magellanic Cloud with the *Einstein* satellite (Long, Helfand, & Grabelsky 1981). The all-sky X-ray survey that was recently carried out with *ROSAT* has now established these supersoft X-ray sources as a distinct class. The known supersoft sources include eight in the LMC, five in the SMC, four in our Galaxy, and more than 15 in M31 (Greiner, Hasinger, & Kahabka 1991; Schaeidt, Hasinger, & Truemper 1993; Hasinger 1993, private communication; Hertz, Grindlay, & Bailyn 1993; Orio & Ögelman 1993). The characteristic photon energies emitted by supersoft X-ray sources are about a factor of 100 times lower than for more conventional X-ray binaries. Two of the supersoft sources have well-studied optical counterparts in the LMC. One of these is CAL 83 with $V \sim 17$ and an orbital period of 1.04 days (Smale et al. 1988; Pakull et al. 1988), while the other is CAL 87 with $V \sim 19$ and with an orbital period of 10.6 hr (Naylor et al. 1989; Callanan et al. 1989; Cowley et al. 1990).

A particular model for at least a large subset of these systems invokes steady nuclear burning of accreted matter on the surface of a $\sim 1\ M_\odot$ white dwarf from a main-sequence or subgiant companion star of ~ 1.3–$2.7\ M_\odot$ (van den Heuvel et al. 1992; Rappaport, Di Stefano, & Smith 1994; and references therein). Mass transfer rates of between 1 and $4 \times 10^{-7}\ M_\odot$ yr^{-1} are required to sustain the luminosity. Such high transfer rates are a natural consequence of unstable mass transfer via Roche lobe overflow in this type of system. The transfer is unstable because the donor star is more massive than the accreting white dwarf; however, the rate of transfer is limited by the thermal time scale of the main-sequence donor star.

Models for the evolution of these systems (Rappaport et al. 1994) indicate that the orbital periods should lie in the range of 8 hr to 1.4 days. Moreover, these studies predict that there should be some 10^3 such systems in the Galaxy and in M31. In spite of the greater distance, it is apparently easier to detect these supersoft sources (at least in the soft X-ray band) in nearby external galaxies at relatively high b^{II}, such as the LMC ($-33°$) and M31 ($-21°$), than it is in the plane of our own Galaxy because a hydrogen column density of only $\sim 10^{21}$ cm^{-2} will absorb most of the very soft X-radiation. In the Galactic plane this corresponds to distances of less than 1 kpc.

Regardless of what the correct model is for the supersoft X-ray sources, it is clear that they emit copious quantities of highly ionizing photons in the range 20–200 eV. Thus, we expect that there will be an ionization nebula surrounding these sources. Unlike a classic H II region, however, where the higher energy photons are absorbed and provide the ionization, while the lower energy photons escape, in the case of the supersoft sources it is the lower energy photons that do the ionizing and the higher energy photons that escape. There should be substantial regions where He is doubly ionized since $\sim 98\%$ and 85% of the radiation (energy) typically lies above the ionization edges of He (24.6 eV) and He$^+$ (54.4 eV), respectively. At the same time, approximately half of the radiation has photon energies less than 100 eV, which assures that it will stop within a few tens of parsecs of the source. Moreover, one expects that the boundary of this type of nebula will be less sharply defined than in a classical H II region since there is substantial power in photons with energies (100–300 eV) that are able to reach moderate and even arbitrarily large distances from the source.

[1] Department of Physics, and Center for Space Research, Massachusetts Institute of Technology, Cambridge, MA 02139.
[2] NASA/Goddard Space Flight Center, Code 665, Greenbelt, MD 20771.
[3] Center for EUV Astrophysics, University of California at Berkeley, CA 94720.

With regard to observational evidence for such ionization nebulae, we point out that Smale et al. (1988) detected extended [O III] emission within their spectrograph slit during observations of CAL 83, but did not detect He II or Hβ. We believe, however, that they were premature in their conclusion that there is no circumstellar nebula, especially since we find in the present work that the ratio of these line intensities can be large (see § 3). By contrast, we note that the X-ray ionized nebula surrounding LMC X-1 found by Pakull & Angebault (1986), while perhaps similar in some respects to the type of nebula we investigate here, is significantly different in the following respects: (1) the optical companion is thought to be a luminous O7 star which produces its own H II region, and (2) its X-ray spectrum (above 1 keV) is very hard compared to the supersoft X-ray sources, and it is difficult to predict what the lower-energy ionizing flux from this source should be.

In § 2 we review the XSTAR computer code that was used to explore the physical properties of the ionization nebulae surrounding supersoft X-ray sources. In § 3 we describe the model calculations that were carried out for a range of source temperatures, source luminosities, and densities for the surrounding interstellar medium. We show sample ionization profiles for hydrogen and helium, and contrast these with the corresponding profiles for a conventional H II region. A table of the prominent optical lines and their intensities that are to be expected from ionization nebulae surrounding supersoft sources is also given in § 3. Discussions and conclusions are presented in § 4.

2. XSTAR CODE FOR COMPUTING IONIZATION STRUCTURE

Our models for ionized nebulae are calculated with the XSTAR computer code (Kallman & Krolik 1993) which uses the computational methods described by Kallman & McCray (1982). In this section we briefly summarize the most important points; more details may be found in the references cited above. The models consist of a spherical gas cloud with a point source of continuum radiation at the center. The input parameters include the source spectrum, the gas composition and density, the initial ionization parameter (which determines the initial radius; see below for a definition), and the column density of the cloud (which determines the outer radius). Construction of a model consists of the simultaneous determination of the state of the gas and the radiation field as a function of distance from the source. The state of the gas at each radius follows from the assumption of a stationary local balance between heating and cooling and between ionization and recombination.

When the gas is optically thin, the radiation field at each radius is determined simply by geometrical dilution of the given source spectrum. Then, as shown by Tarter, Tucker, & Salpeter (1968), the state of the gas depends only on the ionization parameter, proportional to the ratio between the radiation flux and the gas density. We adopt the definition for the ionization parameter used by Tarter et al. (1968): $\xi = L/(nr^2)$, where L is the ionizing luminosity of the central source (between 1 and 1000 Ryd), n is the gas density, and r is the distance from the source. This scaling law allows the results of one model calculation to be applied to a wide variety of situations. For a given choice of spectral shape this parameter is proportional to the various other customary ionization parameter definitions: (1) $U_{\rm H} = F_{\rm H}/n$, where $F_{\rm H}$ is the incident photon number flux above the hydrogen Lyman limit; (2) $\gamma = F_\nu(\nu_{\rm L})/(2hcn)$, where $F_\nu(\nu_{\rm L})$ is the incident (energy) flux at the Lyman limit, and h and c are Planck's constant and the speed of light, respectively; and (3) $\Xi = L/(4\pi r^2 cnkT)$, where T is the electron kinetic temperature, and k is Boltzmann's constant.

This simple picture breaks down when the cloud optical depth is nonnegligible, since the source spectrum then depends on position, and the escape of cooling radiation in lines and recombination continua depends on the total column density of each ion species and hence on the ionization state of the gas throughout the cloud. In this situation the locations of the ionization fronts of hydrogen and helium, and possibly other important ions are given approximately by the Strömgren formula (see, e.g., Dyson & Williams 1980). However, the distribution of ionization of other trace ions and the emissivities of many lines involving temperature sensitive rates do not scale in a simple way. In this case the ionization parameter is still useful in describing the conditions in the innermost regions of the nebula where the ionizing radiation is not yet attenuated significantly.

The state of the gas is defined by its temperature and by the ion abundances. All ions are predominantly in the ground state and, except for hydrogen and helium, the populations of excited levels may be neglected. The relative abundances of the ions of a given element are found by solving the ionization equilibrium equations under the assumption of local balance, subject to the constraint of particle number conservation for each element. Ionization balance is affected by a variety of physical processes, most notably photoionization and radiative and dielectronic recombination. The temperature is found by solving the equation of thermal equilibrium, in which the net heating of the gas due to absorption of incident radiation is equated with the cooling due to emission by the gas. These rates are derived from integrals over the absorbed and emitted radiation spectra. Although Compton scattering is not explicitly included as a source or sink of radiation its effect is included in the calculation of thermal balance.

The emitted spectrum includes continuum emission by bremsstrahlung and recombination, and line emission by a variety of processes including recombination, collisions, and fluorescence following inner shell photoionization. Line transfer is treated using an escape probability formalism, and includes the effects of line destruction by collisions and continuum absorption. Transfer of the continuum is calculated using a single-stream approximation, as described in Kallman & McCray (1982).

Rates for atomic processes involving electron collisions have been modified since the publication of Kallman & McCray (1982) in order to be consistent with those used by Raymond & Smith (1976). In addition, we have added many optical and UV lines from ions of medium-Z elements (C, N, O, Ne, Si, and S) using collisional and radiative rates from Mendoza (1982). The elements Mg, Ar, Ca, and Ni have also been added.

3. CALCULATIONS OF IONIZATION NEBULAE

A series of six models was utilized to study both the H and He ionization profiles and the optical line emissions of regions surrounding supersoft X-ray sources. Each model is characterized by three input parameters: the effective temperature of the supersoft X-ray source, T, the source luminosity, L, and the hydrogen number density, n, of the surrounding interstellar medium (ISM). The input parameters for the six models are summarized in Table 1. Models 1–5 are for ionization regions surrounding supersoft sources, while model 6 is of a classical H II region which we include for purpose of comparison. Input

TABLE 1

SUPERSOFT X-RAY SOURCE MODEL PARAMETERS

Model	T (K)	L (ergs s^{-1})	n (cm^{-3})
1.....	4×10^5	1×10^{38}	10
2.....	2×10^5	1×10^{38}	10
3.....	7×10^5	1×10^{38}	10
4.....	4×10^5	1×10^{37}	10
5.....	4×10^5	1×10^{38}	1
6.....	4.6×10^4	5.1×10^{38}	10

parameters for the latter are taken from the standard H II region model of Evans & Dopita (1986). In all models, the central source is taken to be a simple blackbody, and the elemental abundances relative to hydrogen in the ISM are taken from Withbroe (1972).

The X-ray source in our standard model (model 1) has an effective temperature of 4×10^5 K ($kT = 34$ eV) and a luminosity of 1×10^{38} ergs s^{-1}, values that are representative of those cited in the literature for supersoft X-ray sources (Truemper et al. 1991; Greiner, Hasinger, & Kahabka 1991; Schaeidt, Hasinger, & Truemper 1993; Orio & Ögelman 1993; Hertz, Grindlay, & Bailyn 1993). The hydrogen number density in our standard model is taken somewhat arbitrarily to be 10 hydrogen atoms cm^{-3}, but is a plausible value to use in the vicinity of star forming regions (Allen 1973). For each of the other models 2–5, we hold two of the parameters (T, L, or n) fixed with respect to the standard model and investigate the influence of the third parameter on both the ionization profiles and the nebular line emission. In models 2–5 we consider parameter values of $T = 2 \times 10^5$ K, $T = 7 \times 10^5$ K, $L = 1 \times 10^{37}$ ergs s^{-1}, and $n = 1$ cm^{-3}, in that order.

We present in Figure 1 the H and He ionization profiles calculated for the standard model. The fractional abundance of each ionic species of H and He, that is, the ratio of the abundance of an ionic species to the abundance of its parent element, is shown as a function of radial distance from the source (Figs. 1*a* and 1*b*). The H^+ and H^0 profiles cross at a radius of 6.3 pc with, by definition, each species having a fractional abundance of 50% at that radius. The He^{+2} and He^0 profiles cross at a radius of 6.6 pc with a fractional abundance of 28% each. Approximately centered on this crossing point, there is a broad shell of He^{+1} that reaches a peak fractional abundance of 47%. The calculated temperature profile of the ionized medium is shown in the bottom panel of Figure 1. The temperature drops precipitously to 2×10^4 K within a distance of ~ 1 pc from the central source. Beyond this radius the temperature falls more slowly, but still monotonically, down to $\sim 10^4$ K at the ionization fronts.

In order to characterize both the radial extent of the ionization profiles and the "softness" of the ionization fronts we first define a few terms. We take the quantities R_{H0}, R_{He0}, and R_{He+2} to be the radii at which these subscripted species comprise 50% of their total parental abundance, respectively. The quantities R_{H0} and R_{He0} represent the spatial locations of the transitions between the interior ionized H and He, respectively, and the neutral interstellar medium. Equivalently, these can be taken as roughly the respective radii of the spheres of ionized hydrogen and ionized helium. For our standard model these quantities have values of 6.3 and 7.6 pc, respectively. The quantity R_{He+2} can be considered to be the location of the $He^{+2} \rightarrow He^{+1}$ transition shell which surrounds the innermost

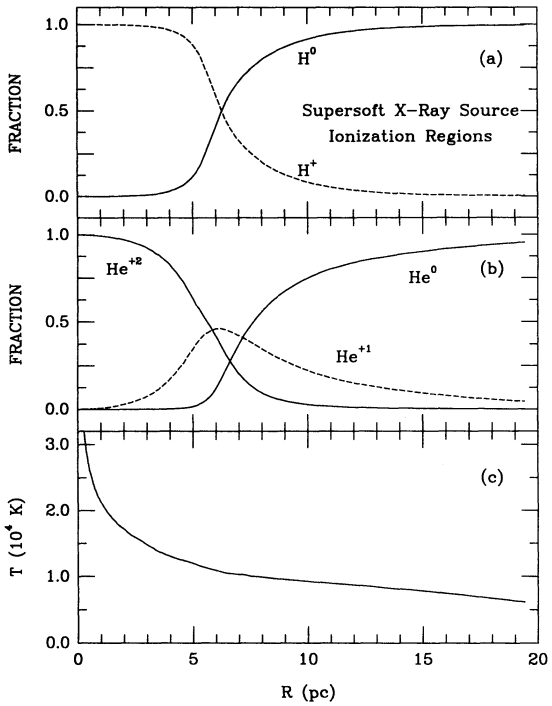

FIG. 1.—Calculated profiles of the ionization region surrounding a supersoft X-ray source for the standard model ($T = 4 \times 10^5$ K, $L = 10^{38}$ ergs s^{-1}, and $n = 10$ cm^{-3}; see text). (*a*) Fractional abundances of neutral and ionized hydrogen. (*b*) Fractional abundances of neutral, singly ionized, and doubly ionized helium. (*c*) Temperature profile.

core that contains most of the doubly ionized helium; it has a value of 5.6 pc in our standard model.

Further, we define the following three quantities: ΔR_{H0}, ΔR_{He0}, and ΔR_{He+2}, to be the radial distances over which the fractional abundances of the subscripted species change from 0.2 to 0.8. These distances are to be interpreted as the thicknesses of each boundary transition shell. The dimensionless quantities $\Delta R_{H0}/R_{H0}$ and $\Delta R_{He0}/R_{He0}$, then, are measures of the "softness" of the hydrogen and helium ionization fronts, respectively, while $\Delta R_{He+2}/R_{He+2}$ quantifies the softness of the boundary of the He^{+2} inner core. These three softness parameters are 0.42, 0.60, and 0.50, respectively, in the standard model. The spherical shell which lies outside the He^{+2} core and which contains most of the singly ionized helium requires different parameters for characterization. We take the radial location of the peak of the He^{+1} profile to be R_{He+1}, and the value of the fractional abundance at maximum to be $f_{He+1,max}$. The former quantity is at 6.2 pc in the standard model. Finally, in this regard, we also define $\Delta R_{He+1}/R_{He+1}$ as the fractional thickness of the He^{+1} shell at 50% of its maximum value (0.87 in the standard model).

Table 2 summarizes the calculated values of the above quantities for the case of the standard model as well as for four other models (see Table 1) that we have calculated. We find that qualitatively, the ionization profiles for all five models look rather similar, except for a radial scaling factor. A perusal of Table 2 indicates expected trends in scale size of the ionization regions with source temperature, source luminosity, and density of the ISM. We derive from the results in Table 2 (and other supplementary models that we have run) the following approximate relation which describes the dependence of R_X on

TABLE 2

CHARACTERISTICS OF IONIZATION ZONES SURROUNDING SUPERSOFT X-RAY SOURCES

Parameter	Model 1	Model 2	Model 3	Model 4	Model 5	Model 6
R_{H0} (pc)	6.28	7.55	5.39	2.81	27.9	14.9
R_{He0} (pc)	7.64	8.03	6.73	3.69	36.8	12.2
R_{He+2} (pc)	5.65	5.62	4.31	2.32	23.2	0.52
R_{He+1} (pc)	6.21	6.99	5.02	2.48	24.7	n/a
$\Delta R_{H0}/R_{H0}$	0.42	0.13	0.74	0.55	0.55	0.013
$\Delta R_{He0}/R_{He0}$	0.60	0.17	0.89	0.77	0.78	0.034
$\Delta R_{He+2}/R_{He+2}$	0.50	0.35	0.68	0.76	0.76	n/a
$\Delta R_{He+1}/R_{He+1}$	0.87	0.38	1.25	1.26	1.27	n/a
$f_{He+1,max}$	0.47	0.84	0.47	0.49	0.49	1.00

the density, the luminosity, and the temperature of the ISM, where X can be any one of the subscripts H^0, He^0, and He^{+2}:

$$R_X \propto n^{-0.65} L^{0.35} T^{0.27} . \quad (1)$$

In this expression, the temperature dependence holds only for zones of H; the radii of the He zones have a somewhat more complicated (but still weak) dependence on T. Simple back-of-the-envelope calculations yield scaling exponents of approximately $-\frac{2}{3}$, $\frac{1}{3}$, and $-\frac{1}{6}$ for the dependence on n, L, and T, respectively.

The ionization and temperature profiles for a conventional H II region are shown in Figure 2 for comparison. As mentioned above, input parameters for this model are taken from the standard H II–region model of Evans & Dopita (1986). Briefly, the parameter values for this model are $L = 5.1 \times 10^{38}$ ergs s^{-1}, $T = 5 \times 10^4$ K, and $n = 10$ cm^{-3}, respectively. Our models differ from those of Evans & Dopita (1986) in that they use a realistic stellar spectrum to represent the source of ionizing radiation while we use a simple blackbody spectrum. Furthermore, although we employ the same excitation rates for most of the strong nebular lines, many of the rates affecting the ionization and thermal balance are undoubtedly different. These include the rates for dielectronic recombination, and the photoionization cross sections. For these reasons we do not expect, nor do we find, exact agreement between our models and those of Evans & Dopita. For example, we find the He I ionization front slightly inside the H I ionization front, whereas Evans & Dopita found them to be coincident. This is likely due to differences in the ionizing spectrum we assume. Nevertheless, we are confident that our models are sufficiently accurate for the purpose of illustrating the important differences between H II regions and nebulae surrounding supersoft sources. With this caveat in mind, we proceed with such a comparison.

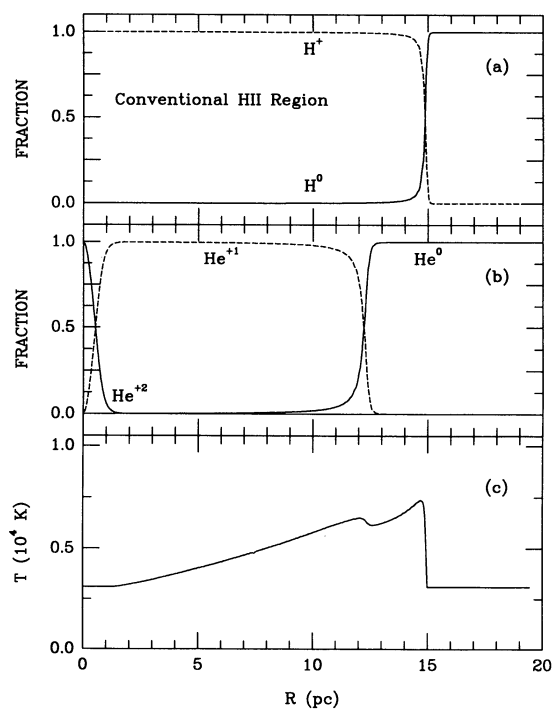

FIG. 2.—Calculated profiles of the ionization regions within a conventional H II region (model 6; $T = 4.6 \times 10^4$ K, $L = 5.1 \times 10^{38}$ ergs s^{-1}, and $n = 10$ cm^{-3}; see text). (*a*) Fractional abundances of neutral and ionized hydrogen. (*b*) Fractional abundances of neutral, singly ionized, and doubly ionized helium. (*c*) Temperature profile.

We find that the radial extent of the ionized medium in our H II region is of the order 15 pc, only somewhat larger than that of our supersoft models, when scaled for the higher luminosity according to equation (1). The most obvious differences of this model with that of the ionization structure surrounding a supersoft X-ray source are (1) the sharpness of the ionization boundaries; (2) the absence of a substantial zone of He^{+2}; and (3) the fact that the H^0 profile lies outside of the He^0 profile. The characteristics of the ionization profiles for the H II region are summarized in Table 2 under the heading of model 6. In general, in regions surrounding supersoft sources the fractional abundances of ionic species of H and He change more gradually with radial distance, i.e., the ionization fronts are "softer" and there is a less obvious demarcation between ionized and neutral regions. By contrast, note that the softness parameters, $\Delta R_{H0}/R_{H0}$ and $\Delta R_{He0}/R_{He0}$, for the H II region have values of only 0.013 and 0.034, respectively; these are more than an order of magnitude smaller than those for our supersoft models. Also note that in the conventional H II region, the plasma temperatures are lower and actually increase with radial distance out to the ionization front.

The source and transmission spectra of the standard model are presented in Figure 3. The source spectrum is simply taken to be a blackbody with $T = 4 \times 10^5$ K. The transmitted photon energy spectrum is evaluated at a radius of ~ 20 pc, near the effective "edge" of the ionized medium. As expected, the continuum luminosity at the edge of the nebula follows the source spectrum at low energies (< 13.6 eV) closely until it drops sharply at the ionization edge of H, remaining very low for energies up to ~ 150 eV. This energy range encompasses the ionization edges of He^0 and He^{+1}. Photons of energy ~ 150–300 eV are also absorbed, but the absorption becomes

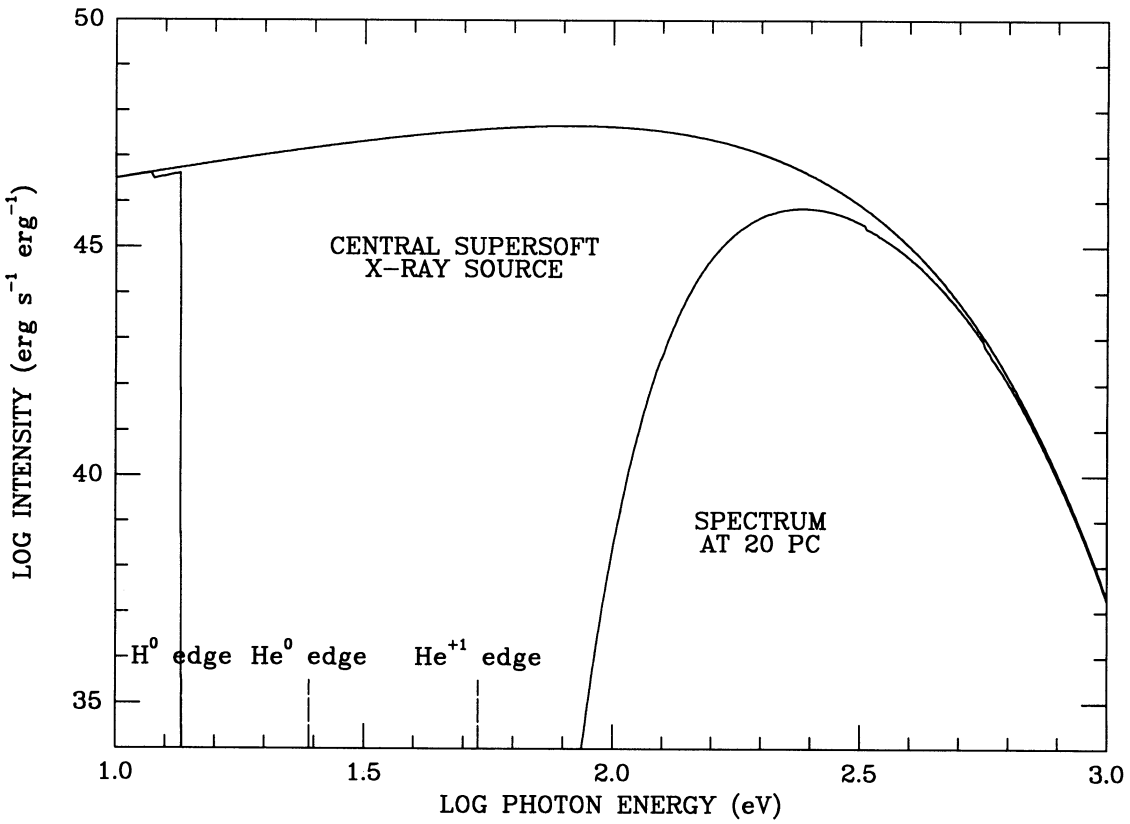

FIG. 3.—Spectrum of the central supersoft X-ray source very near the source and at a distance of 20 pc (beyond most of the ionization regions), for the case of the standard model. Ionization-edge energies for H and He are indicated for reference purpose.

noticeably less efficient with increasing photon energy, consistent with the dependence of the photoelectric absorption cross section on energy. Finally, photons having energies greater than ~300 eV undergo little absorption in the vicinity of the ionization nebula.

Table 3 displays for each of the six model nebulae our calculations of the emission-line fluxes received at Earth. We have evaluated the total power output in each line at the effective "edge" of the ionized medium, defined to be the radial distance by which H and He are each more than ~95% neutral, and the strong lines of N, O, and S have developed their full luminosity. We have taken the distance to the source for every model to be 55 kpc (approximately the distance to supersoft sources in the LMC). No absorption or scattering of the radiation past the boundary of the nebula was considered. We have selected only optical lines (4000–9000 Å) having fluxes greater than 1×10^{-14} ergs cm^{-2} s^{-1}. In addition, we present in Table 4 the individual line luminosities, for each of the six models, normalized to the total source luminosity of the particular model. We selected only those lines from Table 3 having normalized luminosities greater than 10^{-5} [0.001%]. This table makes intercomparison of line strengths among different models more meaningful when the source luminosities are different.

From Table 4 we see that the most prominent lines that are calculated for our standard model (1) of a nebula surrounding a supersoft X-ray source are the Balmer lines, He II λ4686, and the doublets [N I] λλ5202, 5199, [N II] λλ6585, 6550, [O I] λλ6302, 6366, [O III] λλ5008, 4960, and [S II] λλ6718, 6733. Among these emissions, the brightest are [O III], [N II], and [O I] doublet lines which radiate away 4.5%, 2.4%, and 1.9%, respectively, of the total luminosity of the central source. The following lines have substantially larger normalized luminosities in our standard model than in the model H II region: He II λ4686 (> × 100); [N I] λ5202 (× 37); [O I] λ6302 (× 45); [O II] λλ7322 (× 10); and [O III] λ5008 (× 7), where the enhancement factors are shown in parentheses. In contrast, the normalized luminosities of the hydrogen lines are lower than those of a classical H II region by a factor of ~5, as are He I λ6678, [S II] λ6718; Ca I λ4227 is reduced even more.

A number of line-intensity ratios should also be markedly different in a nebula surrounding a supersoft X-ray source as compared to those in a classical H II region. Examples include [O III] (λ5008)/Hβ {12 vs. 0.34}, He II (λ4686)/Hβ {0.47 vs. <0.001}, [O I] (λ6302)/Hβ {5 vs. 0.02}, and [N II] (λ6585)/Hβ {6.4 vs. 1.2}, where the number in brackets are for the standard supersoft model and the model H II region, respectively. The Hα/Hβ ratio is very similar in both models {2.82 vs. 2.73}, as expected. We note that the values of some line ratios from H II region models can vary by as much as an order of magnitude on either side of the most probable values, depending on the differences in input abundances, ionization parameter, and spectral temperature. In the following section, however, we demonstrate that nebulae surrounding supersoft sources are unique in their line ratios, and that the trends in comparative line strengths indicated above are representative of an ensemble of models.

In computing these intensity ratios we have integrated the line luminosities over the entire nebula (i.e., at least out to radial distances where 99% of the line luminosity has

TABLE 3

FLUXES[a] OF PROMINENT OPTICAL LINES SURROUNDING SUPERSOFT X-RAY SOURCES

Wavelength (Å)	Ion	Model 1	Model 2	Model 3	Model 4	Model 5	Model 6
6563	H I	237.7	394.8	180.3	22.6	217.2	6213.0
4862	H I	84.2	140.2	64.1	8.0	77.2	2277.0
4335	H I	40.1	66.9	30.6	3.8	36.9	1119.0
4105	H I	20.7	34.6	15.8	2.0	19.1	591.6
5876	He I	6.9	11.2	7.6	...	8.4	90.6
6678	He I	25.0	38.9	29.0	3.4	32.3	518.1
4686	He II	39.4	41.0	22.4	3.5	33.6	...
6595	He II	4.9	4.9	2.8	...	4.2	...
5202	[N I]	121.2	25.5	296.1	17.2	168.1	17.0
5199	[N I]	81.4	17.1	198.4	11.6	112.5	11.3
6550	[N II]	182.6	187.1	152.2	19.3	185.0	911.4
6585	[N II]	537.6	551.1	448.2	56.9	544.8	2684.0
5756	[N II]	11.4	10.8	9.4	1.1	10.8	12.5
6366	[O I]	138.6	36.2	319.8	19.7	191.3	15.7
6302	[O I]	420.9	109.9	970.8	59.7	580.5	47.7
5579	[O I]	5.0	1.4	9.5	...	6.1	...
7322.4	[O II]	21.6	20.3	19.0	2.1	19.8	10.5
7333	[O II]	11.3	10.6	10.0	1.1	10.4	5.5
7321.8	[O II]	7.2	6.7	6.3	...	6.6	3.5
7332	[O II]	11.9	11.1	10.5	1.1	10.9	5.7
4960	[O III]	349.2	841.2	149.9	23.5	227.5	265.7
5008	[O III]	1006.0	2422.0	432.0	67.6	655.2	765.3
4364	[O III]	15.8	26.2	12.2	1.0	10.2	...
8807	Mg I	...	1.2	3.7	...	1.4	...
4587	Mg I	...	...	4.8	...	1.4	...
4130	Si II	1.1	...	...	...	...	...
6718	[S II]	43.0	29.0	7.5	6.8	66.1	967.5
6733	[S II]	29.3	19.8	5.1	4.6	44.9	664.8
4070	[S II]	1.1	1.2	...	...	1.4	28.6
4077	[S II]	...	...	...	...	...	9.4
6312	[S III]	18.4	1.8	24.9	1.7	16.1	10.1
4227	Ca I	...	...	1.7	...	1.4	16.3

[a] Fluxes are in units of 1×10^{-14} ergs s^{-1} cm^{-2}, for an assumed distance of 55 kpc.

developed). In the special case of the [O III] (λ5008)/Hβ ratio, however, we have also evaluated this quantity over a more limited portion of the nebula where the [O III] (λ5008) line is actively produced. As discussed below, this line is formed over a relatively narrow radial interval when compared with the other nebular lines. Therefore, in citing line ratios involving [O III], one should specify the radial distance over which the ratio has been evaluated. As an example, when integrated over the entire nebula, [O III] (λ5008)/H$\beta \simeq 12$; by contrast, when evaluated only out to radial distances of $\sim 0.68 R_{\rm H0}$, this ratio reaches its maximum value of 26.

We can also compare the normalized line luminosities among supersoft X-ray source models (Table 4). In particular, we note that many of the line luminosities vary systematically with source temperature, T. For example, the Hα and Hβ line luminosities drop by a factor of ~ 2 as T goes from 2×10^5 to 7×10^5 K. We also find that the [O III] lines drop by a factor of ~ 6, while the [O I] lines increase by almost an order of magnitude over the same temperature range. By contrast, the He II and S II line intensities show a less clear trend with source temperature. When the source luminosity and/or the density of the interstellar medium are changed (models 4 and 5) the normalized luminosities of hydrogen, [O III], [O I], and [N II] do not exhibit much variation, as can be readily understood. As the luminosity of the central source is changed, at a fixed source temperature, one expects essentially the same physical processes to occur since the atomic physics reactions that take place are largely governed by the spectral shape of the ionizing radiation rather than by its intensity. In the case of a lower density for the interstellar medium (model 5), we expect the nebula to grow in size but, again, the physical processes in the nebula should reflect more the spectral shape of the ionizing radiation than the density.

We have also examined the spatial distribution of the line radiation within the nebulae, by generating differential and integrated luminosity profiles for five prominent emission lines {Hα, Hβ, [O III] λ5008, [N II] λ6585, and He II λ4686}. In Figure 4*a* we plot the luminosity generated per radial interval for each of the selected lines. Figure 4*b* shows the integrated line luminosity for each of the lines vs. radial distance. We observe, in addition to the aforementioned extremely large power output of the [O III] line, that the spatial extent of the [O III] emission is smaller than those of the other emissions. Approximately 90% of the luminosity from [O III] comes from within a sphere of radius 4.9 pc, whereas the more extended emissions of [He II], [N II], Hα, and Hβ, have corresponding radii of 6.6, 7.2, 7.5, and 7.5 pc, respectively. In fact, if we adopt 4.9 pc as the radius of the [O III] emission region, we find that approximately half of the Hα and Hβ emission comes from outside this region. From these and similar observations (discussed above), it becomes clear that in computing line intensity ratios, it is necessary to specify the radial distance over which the line luminosities are being integrated. As a last note, we observe that the maxima of the differential luminosity profiles for [O III], He II, Hα, Hβ, and [N II] occur at radii of 3.9, 4.8, 5.1, 5.1, and 5.3 pc, respectively.

Finally, we have utilized the differential luminosity profiles shown in Figure 4*a* to compute the expected nebular surface brightness profiles for various emission lines. The surface brightness profiles in Hα, Hβ, and He II all peak at the center of

TABLE 4

NORMALIZED LUMINOSITIES[a] OF PROMINENT OPTICAL LINES

Wavelength (Å)	Ion	Model 1	Model 2	Model 3	Model 4	Model 5	Model 6
6563	H I	0.792	1.316	0.601	0.754	0.724	4.053
4862	H I	0.281	0.467	0.214	0.268	0.258	1.485
4335	H I	0.134	0.223	0.102	0.128	0.123	0.730
4105	H I	0.069	0.115	0.053	0.066	0.064	0.386
5876	He I	0.023	0.037	0.025	...	0.028	0.059
6678	He I	0.083	0.130	0.097	0.112	0.108	0.338
4686	He II	0.131	0.136	0.075	0.116	0.112	...
6595	He II	0.016	0.016	0.009	...	0.014	...
5202	[N I]	0.404	0.085	0.987	0.575	0.560	0.011
5199	[N I]	0.271	0.057	0.661	0.386	0.375	0.007
6550	[N II]	0.609	0.624	0.507	0.644	0.617	0.594
6585	[N II]	1.792	1.837	1.494	1.898	1.816	1.751
5756	[N II]	0.038	0.036	0.031	0.038	0.036	0.008
6366	[O I]	0.462	0.121	1.066	0.655	0.638	0.010
6302	[O I]	1.403	0.366	3.236	1.989	1.935	0.031
5579	[O I]	0.017	0.005	0.032	...	0.020	...
7322.4	[O II]	0.072	0.068	0.063	0.070	0.066	0.007
7333	[O II]	0.038	0.035	0.033	0.037	0.035	0.004
7321.8	[O II]	0.024	0.022	0.021	...	0.022	0.002
7332	[O II]	0.040	0.037	0.035	0.038	0.036	0.004
4960	[O III]	1.164	2.804	0.500	0.782	0.758	0.173
5008	[O III]	3.353	8.075	1.440	2.252	2.184	0.499
4364	[O III]	0.053	0.087	0.041	0.034	0.034	...
8807	Mg I	...	0.004	0.012	...	0.005	...
4587	Mg I	...	...	0.016	...	0.005	...
4130	Si II	0.004	...	...	...	...	...
6718	[S II]	0.144	0.097	0.025	0.227	0.220	0.631
6733	[S II]	0.098	0.066	0.017	0.154	0.149	0.434
4070	[S II]	0.004	0.004	...	...	0.005	0.019
4077	[S II]	...	...	...	...	...	0.006
6312	[S III]	0.061	0.006	0.083	0.056	0.054	0.007
4227	Ca I	...	...	0.006	...	0.005	0.011

[a] Normalized luminosities are given as percentages of the luminosity of the central source.

the nebula, and then fall off monotonically and smoothly as a function of radial distance. By contrast, the [O III] λ5008 and [N II] λ6585 surface brightness profiles have more of a "doughnut" shape with the brightness at the center of the nebula lower by ~33% than at the radius where the surface brightness is a maximum (at 3 pc in [O III] and 4 pc in [N II]).

4. DISCUSSION AND CONCLUSIONS

The detection of ionization nebulae around any of the known supersoft sources should lead to a better understanding of both the source luminosity and the properties of the surrounding interstellar medium. Detailed studies of an ionization nebula, including radial profiles for a number of different emission lines, can lead to independent estimates of the actual luminosity of the central supersoft X-ray source and possibly its temperature. The X-ray observations mostly constrain the luminosity from below (because of uncertainties in the intervening ISM column density) and, in principle, the luminosities could be considerably higher than the Eddington limit for a 1 $M_\odot$ star. Moreover, in cases where we are viewing the binary system nearly in the orbital plane, the direct view of the X-ray source may be blocked by an accretion disk (see, e.g., Schmidtke et al. 1993). However, the strength of the ionization nebula will depend on how much soft X radiation is able to escape, in all directions, from the immediate environment of the binary system. This could provide a more accurate measure of the X-ray luminosity than can be made by direct X-ray observations since, in a sense, the ISM acts like a giant bolometer.

Studies of ionization zones surrounding supersoft X-ray sources could also shed some light on the evolutionary past of these binary systems (see § 1). In particular, investigations of the density, chemical composition, and inhomogeneities in the surrounding ionization nebulae may reveal evidence for possible matter ejected in the form of a stellar wind from the massive star that was the progenitor of the white dwarf and/or matter ejected during a common envelope phase in which the envelope of the progenitor was stripped off.

The development of efficient techniques for searching for ionization nebulae with properties similar to those presented in this work would represent a new means of discovering supersoft X-ray sources using ground-based observations (i.e., at optical wavelengths). This could lead to the discovery of perhaps the majority of supersoft sources that are otherwise undetectable because of severe attenuation by interstellar gas. Models predict ~1000 supersoft sources in our Galaxy, ~100 in the LMC, and ~3000 in M31 (van den Heuvel et al. 1992; Rappaport et al. 1994). Thus, there should be numerous ionization nebulae with distinct spectral and spatial signatures that are detectable in broad searches of the Galaxy, the Magellanic Clouds, and M31. In this regard, we note that the [O III] line flux from a nebula surrounding a supersoft source in M31 would be $\sim 6 \times 10^{-14}$ ergs s^{-1} cm^{-2}, which could still be detectable.

As a first step in establishing an optical spectral signature for

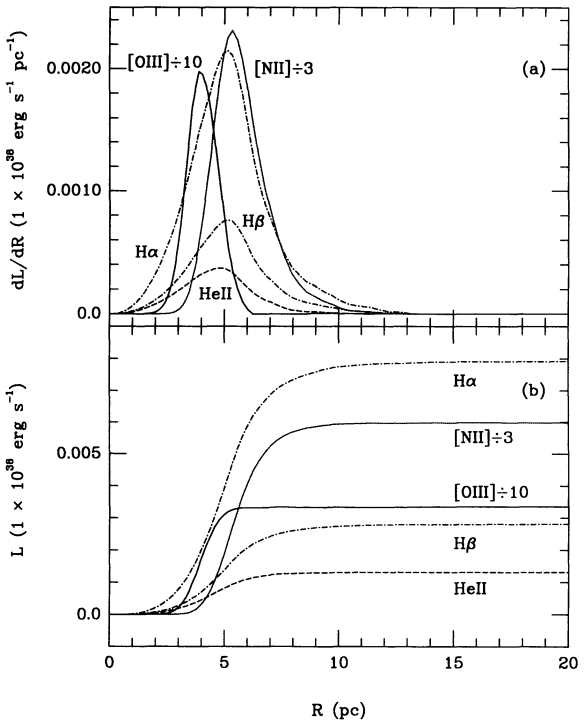

FIG. 4.—Calculated profiles of emission lines {Hα, Hβ, [O III] λ5008, [N II] λ6585, and He II λ4686} within the ionization nebula surrounding a supersoft X-ray source (standard model; $T = 4 \times 10^5$ K, $L = 10^{38}$ ergs s^{-1}, and $n = 10$ cm^{-3}; see text). (*a*) Line luminosity generated per radial interval, dL/dR. (*b*) Integrated line luminosities, $L(<R)$. Note that the curves for [O III] and [N II] have been scaled down by factors of 10 and 3, respectively.

the nebulae surrounding supersoft X-ray sources, we note the potential usefulness of two emission lines, [O III] λ5008 and He II λ4686, which are bright in our supersoft models relative to these same lines in H II regions. In Figure 5, we contrast our supersoft models with various other astrophysical objects in a spectral diagnostic diagram which plots, for a given object, the line-intensity ratio [O III] (λ5008)/Hβ against the ratio He II (λ4686)/Hβ. In this figure, we utilize the maximum in the ratio [O III] (λ5008)/Hβ, which occurs at a radial distance of $\sim 0.65 R_{\rm H0}$, rather than the nebular average of this ratio. We show in the figure a family of supersoft models with source temperatures $kT = 17$ eV (model 2); 34 eV (model 1); 47 eV; and 60 eV (model 3). We do not include supersoft models of varying ISM density or of varying source luminosity because we find that the line ratios are relatively insensitive to these two parameters. Included on the diagram for comparison are a sampled variety of observed astrophysical objects including active galactic nuclei (Shuder 1980; Osterbrock & Pogge 1985; Durret & Bergeron 1986; Osterbrock 1989), supernova remnants (Leibowitz & Danzinger 1983; Osterbrock 1989), planetary nebulae (Aller 1951; Osterbrock 1989), nova shells (Osterbrock 1989), starburst galaxies (Hawley 1978; French 1980; van Breugel et al. 1985; Margon et al. 1988; Sugai & Taniguchi 1992), and H II regions (French 1980). The diagram illustrates the singular nature of supersoft source ionization nebulae as high-excitation objects. Both the uncommonly high He II (λ4686)/Hβ ratio, which ranges from 0.29 to 0.47 for the models considered in the figure, and the unparalleled [O III]/Hβ ratio of ~26, form a distinctive signature for the ionization regions surrounding supersoft X-ray sources.

The results presented in Figures 1–5 and Tables 2–4 are based on an assumed chemical composition for the ISM that is equal to solar abundances (Withbroe 1971). For the specific case of sources in the Magellanic Clouds, however, the metallicities are probably smaller by factors of ~2–8 (Russell & Dopita 1990). In this regard, we have found that a major source of cooling in ionization nebulae surrounding supersoft X-ray sources is provided by [O III]. Therefore, to better understand the possible observational consequences of reduced metallicities, we have rerun our standard model, replacing the input solar abundances with the LMC elemental abundances given by Russell & Dopita (1990); in particular, the oxygen and nitrogen abundances were reduced by factors of 3.2 and 7.8, respectively. All other model parameters remained the same. Qualitatively, we find that the ionization nebula calculated for our reduced-metal model looks very similar to that of our standard model. Quantitatively, we note the following differences. (1) The reduced-metal model has a slightly larger spatial scale: ~10% in $R_{\rm H0}$ and 4% in $R_{\rm He0}$. (2) Comparing the line emissions, we find that our reduced-metal model radiates ~2.2 times less energy in [O III] and [O I] emissions, whereas its hydrogen line emissions are brighter by a factor of ~1.3. The luminosity of He II λ4686 remains high and relatively unchanged. Consequently, the line-intensity ratio [O III] (λ5008)/Hβ falls dramatically from ~26 (standard model) to ~10 (reduced-metal model), while He II (λ4686)/Hβ remains largely unaffected. (3) The intense [N II] λ6585 line in the standard model is weakened substantially (by a factor of ~8) in the reduced-metal model because of the sharp drop in the nitrogen abundance. (4) The temperature profiles of the two models follow each other closely for distances up to ~5 pc, but for greater distances, at and past the ionization fronts, the gas of the reduced-metal model is hotter relative to the standard model, the temperature dropping only slightly to 8×10^3 K at 20 pc. (5) Last, we note that the emission of [S II] λ6718 is highly spatially extended in our reduced-metal model, even more so than for our standard model. We find that 90% of [S II] λ6718 luminosity originates from beyond a radial distance of ~20 pc in the reduced-metal model.

Throughout this work we have taken the density of the medium surrounding the supersoft X-ray source to be a constant in time. In fact, however, the pressure within the ionization nebula will exceed that of the ambient unionized ISM by typically two orders of magnitude. In response to this overpressure the ionized gas expands, driving a shock wave into the neutral ISM which sets it into outward motion. An approximate expression for the expanding radius, R, of the ionized gas sphere as a function of time, t, is given by

$$R(t) \simeq [(7t/4\tau_s) + 1]^{4/7} R_0 \qquad (2)$$

(Dyson & Williams 1980, eq. [7.24]), where R_0 is the radius of the ionized region in the absence of nebular expansion, $\tau_s = R_0/c_s$ is the sound crossing time, and c_s is the sound speed in the ionized region. For parameters appropriate to our problem, $\tau_s \simeq 6 \times 10^5 (R_0/10\ {\rm pc})(T/10^4\ {\rm K})^{-1/2}$ yr. Because of the requirement that the atomic recombination rate within the ionized gas sphere must equal the ionization rate due to the soft X-rays from the central source, the product n^2R^3 must remain approximately constant as the nebula expands (Dyson & Williams 1980; see also eq. [1]). According to equation (2), the ionization nebula will have doubled its size in a time ~1.35 × τ_s or ~10^6 yr, and there will be a corresponding drop in the density by a factor of ~2.8. After 10^7 yr the nebula would have

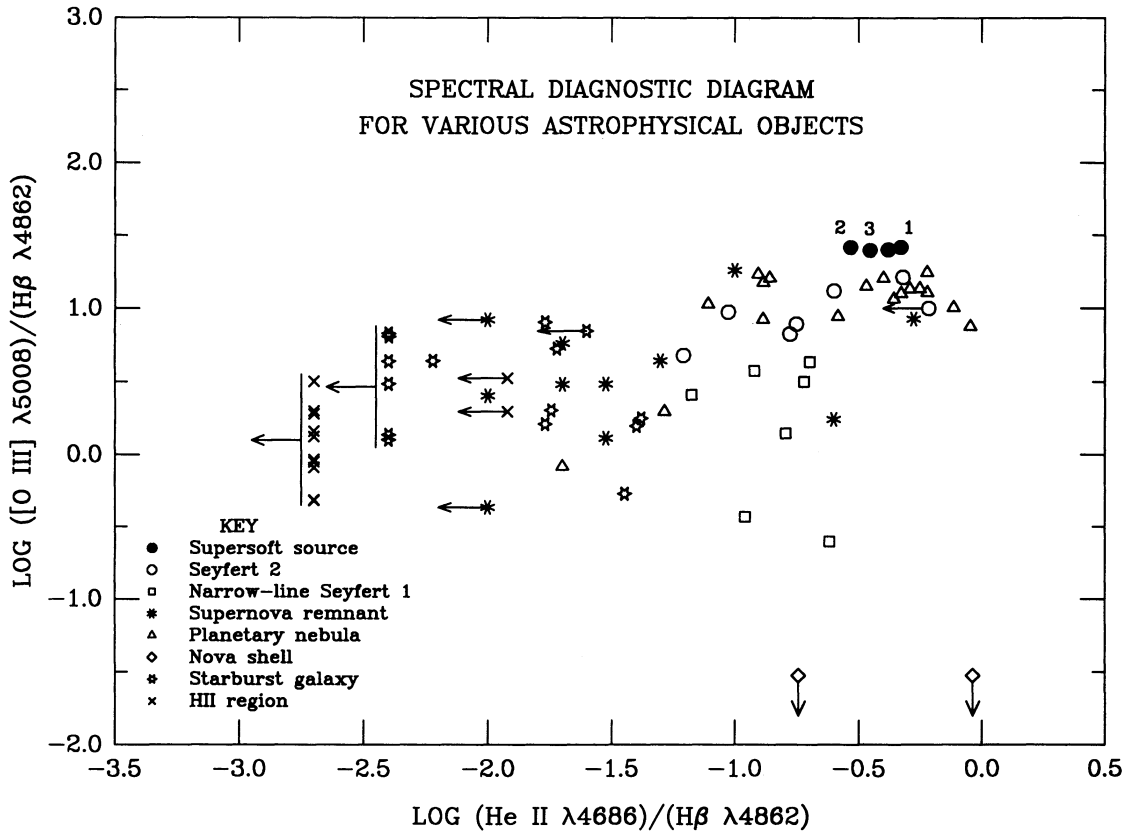

FIG. 5.—Spectral diagnostic line-ratio diagram {[O III] (λ5008)/Hβ vs. He II (λ4686)/Hβ} for supersoft X-ray sources in comparison with other astrophysical gaseous nebulae. Filled circles are the calculated set of line ratios for the case of supersoft X-ray sources (for these objects, [O III]/Hβ has been evaluated at that radial distance in the nebula where this ratio is a maximum, rather than averaged over the nebula; see text.). The numbers near three of the filled circles indicate the model number (see Table 1). Other astrophysical objects are indicated by a variety of symbols which are defined in the inset to the figure. Arrows, in general, represent upper limits; vertical bars with horizontal arrows drawn adjacent to certain starburst galaxies and H II regions indicate common sets of upper limits. Note how the majority of the model supersoft systems lie in a separate region of the diagram toward large values of [O III] (λ5008)/Hβ and He II (λ4686)/Hβ.

expanded by a factor of ~ 7 with a concomitant decrease in the density by a factor of ~ 18. We note that according to the model of van den Heuvel et al. (1992) and Rappaport et al. (1994), the lifetimes of many of the supersoft X-ray sources are expected to be of the order of a few million years. Therefore, there should be at least two likely effects of the expansion of the surrounding nebula. In the first case, the nebula would expand by factors of ~ 2–7 and the density would drop by corresponding factors of ~ 3–20. Based on our model calculations, we expect that such an enlarged radial extent would have relatively little effect on the internal structure of the ionization zones except for an overall scale-size factor (see, e.g., Table 2). However, the larger radial extent would reduce the surface brightness and thereby render these objects more difficult to detect. A second possibility is that the central supersoft X-ray source has a velocity with respect to the ISM that substantially exceeds the sound speed in the ionized region [$c_s \simeq 15\ (T/10^4\ \mathrm{K})^{1/2}$ km s^{-1}]. In this case, the source would "outrun" the expanding nebula and continue to ionize only the matter within a distance R_0; i.e., the size and description of the nebula would be substantially the same as put forth in this work, aside perhaps from a small head-tail asymmetry.

The authors are grateful to R. Remillard for helping us to understand the observational consequences of these calculations and to R. Di Stefano and A. King for extremely useful discussions. This work was supported in part by the National Aeronautics and Space Administration under contract NAS 5-29298 and grant NAGW-1545.

Note added in manuscript.—While this paper was in press, we became aware of reports of an ionization nebula surrounding the supersoft X-ray source CAL 83 (Pakull 1989; Pakull & Motch 1989).

REFERENCES

Allen, C. W. 1973, Astrophysical Quantities (London: Athlone)
Aller, L. H. 1951, ApJ, 113, 125
Callanan, P. J., Machin, G., Naylor, T., & Charles, P. A. 1989, MNRAS, 241, 37
Cowley, A. P., Schmidtke, P. C., Crampton, D., & Hutchings, J. B. 1990, ApJ, 350, 288
Durret, F., & Bergeron, J. 1986, A&A, 156, 51
Dyson, J. E., & Williams, D. A. 1980, Physics of the Interstellar Medium (Toronto: Wiley)
Evans, I. N., & Dopita, M. A. 1986, ApJS, 58, 125
French, H. B. 1980, ApJ, 240, 41
Greinger, J., Hasinger, G., & Kahabka, P. 1991, A&A, 246, L17
Hawley, S. A. 1978, ApJ, 224, 417
Hertz, P., Grindlay, J. E., & Bailyn, C. D. 1993, ApJ, 410, L87
Kallman, T. R., & Krolik, J. H. 1993, preprint
Kallman, T. R., & McCray, R. A. 1982, ApJS, 50, 263
Leibowitz, E. M., & Danzinger, I. J. 1983, MNRAS, 204, 273
Long, K. S., Helfand, D. J., & Grabelsky, D. A. 1981, ApJ, 248, 925

Margon, B., Anderson, S. F., Mateo, M., Fich, M., & Massey, P. 1988, ApJ, 334, 597
Mendoza, C. 1982, in Proc. IAU Symp. 103, Planetary Nebulae, ed. D. R. Flower (Dordrecht: Reidel), 143
Naylor, T., Callanan, P. J., Machin, G., & Charles, P. A. 1989, IAU Circ., No. 4747
Orio, M., & Ögelman, H. 1993, A&A, in press
Osterbrock, D. E. 1989, Astrophysics of Gaseous Nebulae (Mill Valley, CA: University Science Books)
Osterbrock, D. E., & Pogge, R. W. 1985, ApJ, 297, 166
Pakull, M. W. 1989, in Recent Developments of Magellanic Cloud Research, ed. K. S. Boer, F. Spite, & G. Stasinska (Paris: Observatoire de Paris), 183
Pakull, M. W., & Angebault, L. P. 1986, Nature, 322, 511
Pakull, M. W., Beuermann, K., van der Klis, M., & van Paradijs, J. 1988, A&A, 203, L27
Pakull, M. W., & Motch, C. 1989, in Proc. ESO Workshop on Extranuclear Activity in Galaxies, ed. E. J. A. Meurs & R. A. E. Fosbury (Garching: ESO), 285
Rappaport, S., Di Stefano, R., & Smith, J. D. 1994, ApJ, 426, 692
Raymond, J. C., & Smith, B. H. 1976, ApJS, 35, 419
Russell, S. C., & Dopita, M. A. 1990, ApJ, 74, 93
Schaeidt, S., Hasinger, G., & Truemper, J. 1993, A&A, 270, L9
Schmidtke, P. C., McGrath, T. K., Cowley, A. P., & Frattare, L. M. 1993, PASP, 105, 863
Shuder, J. M. 1980, ApJ, 240, 32
Smale, A. P., et al. 1988, MNRAS, 233, 51
Sugai, H., & Taniguchi, Y. 1992, AJ, 103, 1470
Tarter, C. B., Tucker, W. H., & Salpeter, E. E. 1969, ApJ, 156, 943
Truemper, J., et al. 1991, Nature, 349, 579
van Breugel, W., Filippenko, A. V., Heckman, T., & Miley, G. 1985, ApJ, 293, 83
van den Heuvel, E. P. J., Bhattacharya, D., Nomoto, K., & Rappaport, S. A. 1992, A&A, 262, 97
Withbroe, G. 1971, in The Menzel Symposium on Solar Physics, Spectra, and Gaseous Nebulae, NBS SP 353, ed. K. B. Gebbie (Washington, DC: NBS), 127